

UCSF

UC San Francisco Previously Published Works

Title

Disruption to control network function correlates with altered dynamic connectivity in the wider autism spectrum.

Permalink

<https://escholarship.org/uc/item/1rt878dm>

Authors

de Lacy, N
Doherty, D
King, BH
et al.

Publication Date

2017

DOI

10.1016/j.nicl.2017.05.024

Peer reviewed



Disruption to control network function correlates with altered dynamic connectivity in the wider autism spectrum



N. de Lacy^{a,b}, D. Doherty^{b,c}, B.H. King^d, S. Rachakonda^e, V.D. Calhoun^{e,f,*}

^a Department of Psychiatry and Behavioral Sciences, University of Washington, Seattle, WA 98195, USA

^b Seattle Children's Research Institute, Center for Integrative Brain Research, Seattle, WA 98105, USA

^c Department of Pediatrics, Divisions of Developmental and Genetic Medicine, University of Washington, Seattle, WA 98195, USA

^d Department of Psychiatry, University of California San Francisco, San Francisco, CA 94143, USA

^e The Mind Research Network & LBERI, Albuquerque, NM 87106, USA

^f Department of Electrical and Computer Engineering, University of New Mexico, Albuquerque, NM 87131, USA

ARTICLE INFO

Keywords:

Autism
Functional MRI
Dynamic connectivity
Control networks
Task-positive
Default-mode

ABSTRACT

Autism is a common developmental condition with a wide, variable range of co-occurring neuropsychiatric symptoms. Contrasting with most extant studies, we explored whole-brain functional organization at multiple levels simultaneously in a large subject group reflecting autism's clinical diversity, and present the first network-based analysis of transient brain states, or *dynamic connectivity*, in autism. Disruption to inter-network and inter-system connectivity, rather than within individual networks, predominated. We identified coupling disruption in the anterior-posterior default mode axis, and among specific control networks specialized for task start cues and the maintenance of domain-independent task positive status, specifically between the right fronto-parietal and cingulo-opercular networks and default mode network subsystems. These appear to propagate downstream in autism, with significantly dampened subject oscillations between brain states, and dynamic connectivity configuration differences. Our account proposes specific motifs that may provide candidates for neuroimaging biomarkers within heterogeneous clinical populations in this diverse condition.

1. Introduction

Autism spectrum disorder (ASD) is a lifelong neuropsychiatric condition affecting > 1% of the population with a lifetime cost of care of \$1.4–2.4 million (Buescher et al., 2014). Diagnostic criteria specify social communication deficits and restricted/repetitive behavior patterns. However, symptoms extend to most neurocognitive systems (Silver and Rapin, 2012) including prominent visual, language and sensorimotor differences. Co-morbid findings in individuals with autism include intellectual disability (40–50%), seizures (8–30%), neuromotor abnormalities ($\leq 79\%$), sleep disruption (50–80%), and gastrointestinal symptoms (9–70%) (Silver and Rapin, 2012; Lai et al., 2014). Psychiatric comorbidities are strikingly common, most frequently anxiety and attention deficit hyperactivity disorder (ADHD), each present in ~50% (Lai et al., 2014).

ASD may be considered a developmental disorder of distributed neural systems, evidenced by alterations in microscale (Zoghbi and Bear, 2012), mesoscale (Hutsler and Casanova, 2015) and macroscale (Duerden et al., 2012) neural architecture. Current estimates of heritability are 80%, albeit with substantial genetic heterogeneity

(Geschwind and State, 2015) and environmental contributions (Herbert, 2010). While multiple neural elements appear implicated, no consistent or unifying structural or functional motif has been identified and validated. Consequently, ASD remains a taxonomic umbrella term rather than a disease (Silver and Rapin, 2012). Identifying a convergent mechanism capable of reconciling the characteristic infantile onset and core behavioral phenotype with observable neurocognitive diversity and biomolecular heterogeneity remains a fundamental unsolved problem.

ASD research has benefitted from the increasing conceptualization of behavior and cognition as being emergent properties of brain networks. In this model, a network consists of multiple regions or nodes (that may be spatially distant from each other) exhibiting stable, organized patterns of persistent co-activation or coherence when brain function is measured. This patterned co-activation between nodes within a network has been termed *functional connectivity*, and multiple techniques may be used to search for and define networks, including independent component analysis (ICA), seed-based, graph and clustering techniques. There appear to be multiple, stable networks in the human brain present across individuals that have been associated with

* Corresponding author at: The Mind Research Network & LBERI, Albuquerque, NM 87106, USA.
E-mail address: vcalhoun@mrn.org (V.D. Calhoun).

specific behavioral or cognitive functions such as vision (Laird et al., 2011). Interestingly, networks appear to be replicable across conditions, and many have been identified during task performance that correspond to those seen in the wakeful resting state (Smith et al., 2009), anesthesia and sleep (Zhang and Raichle, 2010), suggesting resting state neurocognitive templates are activated during tasks (Spreng et al., 2013). Taken together, these observations also suggest these large-scale networks may be inherent in human brain function, giving rise to the appellation ‘intrinsic network’ (IN) (Seeley et al., 2007). Spatio-temporally patterned, correlated activity also exists between networks, that may be termed *functional network connectivity* (FNC, Fig. 1a). Here, individual networks may be initially defined using a variety of techniques such as ICA or seed-based methods, before defining connectivity characteristics between two or more networks. Commonly, FNC is analyzed by examining successive pairs of networks to eventually compute all the possible relationships among a set of N networks, or $[(N \times N) - N] / 2$. Identification of the total set of brain networks and the character of connections within and between them may therefore provide a map of the human functional ‘connectome’, akin to a whole-brain wiring diagram.

When observed using functional MRI (fMRI) in the resting state, co-activation patterns characterizing functional connectivity and FNC are often averaged across the timecourse of scans, producing measures of steady-state connectivity. Analytic approaches capable of characterizing the time-varying properties of network configurations in fMRI, or *dynamic connectivity*, have recently garnered substantial interest (Calhoun et al., 2014). When their temporal organization is thereby additionally delineated, functional connectivity and FNC together form what we have called the human ‘chronnectome’: a multi-level architecture housed in the same physical substrate but simultaneously allowing functional specialization and the dynamic integration required for complex cognition. Much work remains to be done to provide a detailed description of the role that different individual networks play in dynamic connectivity, and how this could relate to a model where distinct brain ‘states’ may specify shifts in neurocognitive function and behavior such as the redirection of attention. However, while networks are known to specialize, two broad types exist. Domain networks perform specific data processing functions for tasks such as vision, while control networks effect top-down/executive management of process initiation, maintenance and transition via FNC configuration shifts. The functional characterization of control networks and their inter-relationships is therefore of interest in considering dynamic connectivity. Patterns of resting state inter-network FNC can differentiate affected from unaffected individuals in disorders of complex cognition such as depression (Manoliu et al., 2013), obsessive-compulsive disorder (Anticevic et al., 2014), schizophrenia and bipolar disorder (Du et al., 2015). Similarly, ASD is increasingly considered a connectivity disorder (Zhang and Raichle, 2010). However, the specific connectivity deficits have greatly varied given methodological and subject selection differences. Early studies often focused on region-specific differences in activation during tasks, with more recent inquiry using resting state fMRI concentrated in seed-based techniques (Hull et al., 2016) and low-order models. Many studies have focused on smaller groups of more homogenous subjects (often males with higher cognitive function) without psychiatric co-morbidities. However, it is not clear if these more narrowly-defined groups may represent sub-populations within ASD, and the use of restricted numbers of networks may obscure underlying connectivity patterns. In contrast, we opted to perform an exploratory, hypothesis-free study in a large group of subjects of varied ages using resting state fMRI. We embraced – but controlled for – the neurocognitive and psychiatric diversity found in clinical populations with ASD. Using a high-order model to achieve fine spatial and temporal scale, we applied ten advanced outcome measures to this large dataset to maximize power. We were particularly interested in juxtaposing measures at different hierarchical levels of functional brain organization that characterize connectivity within networks, between

networks and at the aggregated network system level and comparing connectivity motifs across steady-state and dynamic FNC.

2. Materials and methods

2.1. Methods summary

After pre-processing with standard techniques in the DPARSF pipeline, resting-state scans from 884 subjects were pre-whitened and a two-step principal components (PC) analysis was performed to reduce to 75 PCs. A high-order 75 component group ICA (gICA) using the Infomax algorithm was run 10 times with random initialization using ICASSO, and subject specific spatial maps estimated using back reconstruction with the GICA algorithm. Measures of intra-network, inter-network and inter-system connectivity in the averaged (steady-state) fMRI timecourses were tested for group effects in autism vs controls, controlling for IQ, age, sex, site, eye status, medication use, co-morbid diagnosis and head motion. In voxelwise outcome measures, predictors were submitted to a MANCOVA with an F-test at each iteration to produce a final reduced model for each outcome measure and network, before univariate testing of significant predictors was performed on the original model. For the dynamic analysis, successive correlation matrices for all networks were generated using a sliding window technique and brain states formed using k-means clustering on the windowed correlation matrices. Dynamic outcome measures including examination of variance in the temporal patterns of subject transition among states were tested in autism vs controls after controlling for site and head motion. A sensitivity analysis was performed using 9 permutations of cluster number and window size. Directional test-retest analysis was performed. A detailed account of Methods follows.

2.2. Data selection and preprocessing

The base data for this study is the collection of MRI scans assembled by the Autism Brain Imaging Data Exchange (ABIDE) consortium from 16 different study sites (Di Martino et al., 2014). Resting state and MPAGE structural data for 1112 subjects (539 with ASD and 573 neurotypical controls) are made available. This data is deidentified in compliance with U.S. Health Insurance Portability and Accountability Act (HIPAA) guidelines and in the public domain. The research was approved by local human subjects committees at all sites and participants signed written informed consents and assents. The present study was given exempt status by the University of Washington Human Subjects Committee. We included in this study only scans that were rated as ‘good’ by two or more of three raters in the ABIDE QI process (see http://preprocessed-connectomes-project.github.io/abide/quality_assessment.html). We then discarded scans with < 110 timepoints in the resting state scan since we wanted to preserve our ability to compute a high order model, and further eliminated 59 subjects for whom IQ data was not available. In total, 884 subjects ages 6.5 to 58 were included, 423 with ASD and 461 controls. Certain subjects were taking psychoactive medications at the time of the scan. Supplementary Table 4 shows characteristics of the subjects in this study.

We utilized resting state scans with minimal processing using the Data Processing Assistant for Resting State fMRI (DPARSF) without band-pass signaling and without global signal regression. The first four volumes were dropped from each scan to remove T1 equilibration effects. Scans then underwent slice time correction in order to correct for different signal acquisition times, shifting the signal measured in each slice relative to the acquisition of the slice, using the middle slice as the reference frame. Subsequently, realignment was performed using a six-parameter (rigid body) linear transformation with a two-pass procedure, first registering to the first image and then to the mean of the images. Structural images (T1-weighted MPAGE) were segmented into gray and white matter (GM and WM) and cerebrospinal fluid (CSF), co-registered to the mean functional image and then transformed from

individual native to Montreal Neurologic Institute 152 space using the Diffeomorphic Anatomical Registration Through Exponentiated Lie algebra (DARTEL) tool. Minimal, standard regressions were performed on the resulting data to ensure the signal used in the analysis represented coactivation responses from GM. Specifically, head motion effects were regressed out using the Friston 24-parameter model and signal from WM and CSF regressed out to remove respiratory and cardiac effects. Finally, linear and quadratic trends were included to account for low frequency drift in the blood oxygen level dependent signal. See <http://preprocessed-connectomes-project.github.io/abide/Pipelines.html> and <http://preprocessed-connectomes-project.github.io/abide/dparsf.html> for additional details. We performed temporal filtering later in our processing pipeline.

2.3. Analytic pipeline

The approaches we adopted in our general analytic pipeline to extract and identify INs and perform static and dynamic connectivity analysis have been developed in our group at the Mind Research Network and validated in large groups of control subjects. Further details of the computational underpinnings may be examined in recent published studies (Allen et al., 2011; Allen et al., 2014). Accordingly, in this section we set forth specific methodologic choices we made in the current analysis to optimize our approach and results given the high dimensionality of the data, large number of subjects and computationally resource-intensive nature of these techniques. Additional outcome measures were developed specific to the present study (Intra- and inter-system correlations, state change number and fraction of time spent in state) and these are described in detail. Software tools used in this analysis are made freely available at: <http://mialab.mrn.org/software>.

2.4. Group independent component analysis

We identified large scale brain networks in the subject sample using a spatial ICA algorithm instantiated in the Group ICA of fMRI Toolbox (GIFT) developed in our group and widely used in ICA analysis of fMRI (Calhoun and Adali, 2012). In this approach, spatial maps representing temporally coherent individual networks are extracted or deconvolved from the linearly mixed whole brain resting state signal by estimating maximally independent spatial sources. The group ICA model assumes that the set of independent source locations have weights specifying the contribution of each source to each voxel, with these weights multiplied by each source's timecourse. The total number of sources are then added together, with each voxel containing a mixture of the sources, each of which fluctuates according to its weighted timecourse with every component making some contribution at each voxel. This may be appreciated in Supplementary Fig. 1 by noting that spatial overlap between networks is present even on visual inspection (for example INs 12/13, 18/19, 20/21, 2/8/9 or 24/26). In addition, we computed the normalized mutual information between each pair of components (Supplementary Fig. 2) to demonstrate the shared information between every component pair in the decomposition.

Each independent component (IC) therefore represents a network extracted *en bloc* from the pooled sample of 884 individuals to maximize component refinement and specificity (Smith et al., 2009; Allen et al., 2011). This is a hypothesis-free, data-driven approach to identifying brain networks that computes relationships between all voxels in the resting state data rather than estimating pairwise correlations, and may provide increased sensitivity to detect subtle intra-subject differences (Calhoun and Adali, 2012).

We performed a group independent component analysis (gICA) using a relatively high order model of 75 components (Zhang and Raichle, 2010; Allen et al., 2011). Before the gICA, we submitted the data to reduction and pre-whitening (the latter to remove effects attributable to serial autocorrelation) in a principal components (PC)

analysis. First, we performed a subject-specific data reduction PC analysis using a standard economy-size decomposition retaining 90 PCs with the objective of stabilizing back reconstruction and retaining maximum variance at the individual level. We next performed group data reduction retaining 75 PCs in order to reduce dimensionality in the data to the number of components used in the ICA. For the second, group data reduction step, we used the expectation-maximization algorithm included in GIFT to maximize performance, removed the mean image per timepoint to improve conditioning of the covariance matrix, and masked data with an ABIDE-specific template derived from a single ABIDE MPAGE scan selected at random. The data was fully stacked to compute the covariance matrix with double point precision. Then we performed the gICA analysis by repeating the Infomax ICA algorithm 10 times in ICASSO (Himberg et al., 2004). In the latter approach the ICA algorithm is run multiple times starting with different, randomly selected initial values to obtain clusters that are the most representative and therefore most reliable estimate for each component. There is currently no idealistic way to specify the number of ICs in an ICA decomposition, but rather choices available to the researcher based on study design preferences and the dimensionality of the data. Automated approaches typically converge on a lower number of components (Li et al., 2007) but over the past few years many studies have manually opted for a higher model order. We selected an intermediate-high (75) number of independent components because we wished to isolate independent right and left fronto-parietal control networks. In this we followed Smith et al. (Smith et al., 2009) and Allen et al. (Allen et al., 2011) who demonstrated using ICA that a high model order is necessary to extract these specific networks. In terms of the number of PCs, we have previously demonstrated (Erhardt et al., 2011) that the performance of the ICA decomposition is insensitive to variations in this parameter, as long as the number of PCs is greater than the number of ICs.

Aggregate spatial maps were estimated as the centrotypes of component clusters to reduce sensitivity to initial algorithm parameters (Ma et al., 2011). Single-subject images were concatenated in time to perform the single group ICA estimation and subject specific spatial maps estimated using back reconstruction with the GICA approach in GIFT. The GICA algorithm estimates single-subject images and timecourses from the single group ICA estimation, thereby allowing individual variation in spatial maps and timecourses (Erhardt et al., 2011), and we have previously demonstrated that inter-subject variance is well-captured in the group ICA model using this algorithm (Allen et al., 2012). The resulting independent components (ICs) were scaled by converting each subject component image and the time course to z-scores. We performed an analysis of the reliability of the ICA source estimates obtained in the ICA decomposition by calculating a stability metric (Ma et al., 2011) for each of the ICASSO clusters (Reported in Supplementary Table 1). This demonstrated that the decomposition achieved compactly clustered components, with > 95% of components achieving > 0.75 average intra-cluster similarity where > 0.7 is considered acceptable. Components with < 0.75 average intra-cluster similarity were discarded to be conservative.

2.5. Network selection and feature identification

ICA generates components from the mixed fMRI signal that represent a mix of 'true' brain networks and artefactual components from various sources such as cerebrospinal fluid, white matter, blood vessels and head motion. The separation of components into these two groups currently remains a semi-manual process, informed by quantitative metrics but reliant on the experience of the investigators, though the automation of this process is an area of ongoing research by ourselves and others. For each of the 75 ICs in this study, we separated INs from artifact by examining spectral metrics and visually inspecting the spatial maps. Spectra were characterized by two metrics: the fractional amplitude of low frequency fluctuations (fALFF), and dynamic range.

fALFF is the ratio of the integral of spectral power below 0.10 Hz to the integral of power between 0.15 and 0.25 Hz. Dynamic range is the difference between the peak power and minimum power at frequencies to the right of the peak. Data are provided for each component in Supplementary Table 2. Generally, ICs that represent brain networks have higher values in spectral metrics, while noise components have lower values. Two graders (NdL and VDC) used the metrics to rate the ICs “good”, “fair” and “poor”. “Poor” components with low spectral values were discarded, with the two components with < 0.75 intra-cluster similarity in the ICASSO analysis also detected in this group. Spatial maps rated “fair” and “good” based on metrics were visually inspected and any considered marginal were also excluded to pursue a conservative analysis. In particular, components with activation that visually overlaps white matter, or has a strong ‘edge like’ appearance were discarded. We retained 33 ICs that were the 33 INs collectively forming the analytic substrate for the remainder of our study (Supplementary Fig. 1).

Maxima of coordinates in MNI space associated with each of the INs are detailed in Supplementary Table 3. An attribution was made of the primary neurocognitive function of each IN using, where available, prior studies defining networks on the basis of specific coordinates and/or regions and also by examining the function of four or more of the highest maxima using the Brodmann Interactive Atlas (<http://www.fmriconsulting.com/brodmann/Interact.html>). Multiple literature-based confirmatory sources with specific Talairach or MNI coordinates were available for all members of the TPN and the DMN (the control INs) and for the primary sensorimotor and visual networks (Laird et al., 2011; Smith et al., 2009; Spreng et al., 2013; Seeley et al., 2007; Dosenbach et al., 2006; Dosenbach et al., 2007; Power et al., 2011; Fox et al., 2005; Vernet et al., 2014). Subsequently, we grouped INs into primary neurocognitive systems, namely task positive (TPN), default mode (DMN), visual (VIS), sensorimotor (SM), language (LANG) and other control (OTH) networks.

2.6. Steady-state functional connectivity measures

We computed 5 outcome measures to characterize steady-state connectivity, summarized in Table 1:

To compute power spectra, subject-specific timecourses were detrended using the multi-taper approach derived from Chronux (Bokil et al., 2010), with the time-bandwidth product set to 3 and the number of tapers set to 5. Spectra were then element-wise log-transformed to normalize the skewed power distribution. We constructed spatial maps by selecting voxels that represented the strongest and most consistent coactivations for each IN on a voxelwise basis across all subjects, by performing a voxelwise one-sample *t*-test on the individual subject component imaging and thresholding individual voxels at (mean + 4 standard deviations). Thus, spatial maps represent the brain regions most associated with the component's timecourses, instantiated in thresholded *t*-maps. We constructed the steady-state FNC matrix by computing the Pearson's correlation coefficient between every pair of timecourses to generate a symmetric 33×33 matrix of correlations for each subject. First, subject-specific timecourses were detrended and despiked, and filtered using a fifth-order Butterworth low-pass filter with a high frequency cutoff of 0.15 Hz. Correlations were then

transformed to z-scores using Fisher's transformation ($z = \text{atanh}(k)$) where k is the correlation between the timecourses of any two components.

Using the Pearson's correlation coefficient between every pair of INs for each subject, we constructed sets of correlations to form the intra-system and inter-system measures. For the intra-system measure, correlations pairs were grouped into the neurocognitive system of interest corresponding to our core grouping of INs. For example, all correlations between each of the possible pairwise combinations of the seven sensorimotor networks comprised the sensorimotor system group. For the inter-system measure, positive and negative correlation pairs were similarly grouped but in this case to examine effects between the systems. For example, the inter-system correlation between the TPN and DMN would include all possible pairings among the six TPN and three DMN INs.

2.7. Steady-state connectivity statistical analysis

Covariates (predictors) of interest (Extended Data Table 4) were age in years, full scale IQ level, framewise displacement (coded as continuous variables), site, male or female sex, diagnosis of autism or controls, whether subjects had their eyes open or closed during the scan, if subjects were on any medication at the time of the scan, and the presence of any co-morbid diagnoses (coded as discrete variables). Data for each subject were obtained from the ABIDE phenotypic file. We were not able to model handedness, since handedness is not available in the ABIDE phenotypic file for many sites. Age and IQ were plotted as histograms and compared with the Gaussian distribution, and skewness and kurtosis calculated, and age was log transformed. Since the dataset includes images acquired from 16 sites, we also included the site where the study was performed as a covariate in order to examine whether site was a significant predictor of response variation. Each site was modeled as an individual regressor. While the variance from all sites was retained, the first site alphabetically (CalTech) was selected to act as a dummy variable (comparison group) within the multiple regression model to avoid exact collinearity. Every possible pair of covariates was submitted to modeling and all effects on outcome measures were analyzed on a voxelwise basis, a more conservative method than cluster-based techniques (Eklund et al., 2016).

In order to optimize for the large dimensions of the voxelwise outcome measures (Spectra, spatial maps and FNC pairwise correlations) we used a multivariate model selection strategy to enable testing of predictors on the response matrices (for voxelwise outcome measures) as a whole and reduce the number of statistical tests performed. First, we proceeded by backward selection, performing a multivariate analysis of covariance (MANCOVA) on each predictor in the model using the MANCOVAN toolbox in GIFT (Allen et al., 2011). This proceeds in a stepwise fashion, performing an F-test at each iteration to compare the current full model with the reduced model and produce a final reduced model in which all terms not associated with higher order interactions are preserved at $\alpha = 0.01$ to control false discovery rate (FDR). Reduced models were independently selected for each voxelwise outcome measure and every IN. In the MANCOVA, site and mean framewise displacement were found to be significant predictors. Accordingly, the variance associated with site and framewise displacement was removed from the analysis by removing the variance associated with each individual site regressor and the framewise displacement regressor from the correlation values.

Subsequently, significant predictors were submitted to multiple univariate regressions and covaried with age, sex, diagnostic group, medication status, presence of psychiatric co-morbidities and IQ. We tested for significance at $\alpha < 0.01$ corrected for multiple comparisons to control FDR to discover which outcome measures were associated with age, sex, diagnostic group, medication status, presence of psychiatric co-morbidities, and IQ. Univariate models were fit to the original data and not the reduced model. For the FNC correlation measures

Table 1
Steady-state outcome measures.

Measure	Hierarchical level and type of characterization
Power spectra	Within-network coherence
Spatial maps	Strongest within-network regional activations
FNC	Pairwise connectivity between individual networks
Intra-system	Correlation strength within grouped networks
Inter-system	Correlation strength between grouped networks

we calculated the standard error of the mean (STDERR). We performed a similar analysis using the same components including only subjects with ASD to further determine if the presence of psychiatric co-morbidities and current use of medication were significant predictors, and found that they were not. In order to assess for residual motion effects, the interaction of framewise displacement \times group was also tested in the univariate analysis to assess for residual motion effects in significant predictors.

For the intra-system measure, we calculated the mean of correlations for all possible pairwise combinations of INs within each system (for example, all the sensorimotor INs). We then performed two sample t -tests (2-tailed, assuming equal variance) to discover whether significant ($\alpha < 0.05$, corrected to control FDR) differences existed for mean intra-system correlations between subjects with autism and controls.

For the inter-system analysis, we calculated mean of correlations for all possible pairwise combinations of INs between pairs system (for example, all the sensorimotor INs with all DMNs). We then performed two sample t -tests (2-tailed, assuming equal variance) to discover whether significant ($\alpha < 0.05$, corrected to control FDR) differences existed for mean inter-system correlations between subjects with autism and controls.

2.8. Dynamic connectivity

We computed dynamic FNC using a sliding window approach instantiated in the dFNC toolbox in GIFT. First, the timecourses were detrended and despiked using 3D despiking in the AFNI software then filtered using a fifth-order Butterworth low-pass filter with a high frequency cutoff of 0.15 Hz. Then, FNC covariance matrices were calculated between all pairwise INs for each subject using the correlations derived from our ICA analysis by moving a Gaussian window in 1 TR increments across the subject TCs. Of note, since this is multisite data the TR varies from site to site with a range of 1.5 to 3 s and our algorithm incorporated this. In addition, the variance associated with site was removed from the analysis by removing the variance associated with each individual site regressor from the correlation values, prior to performing clustering. Successive FNC matrices for each window were then concatenated to form a $[33 \times 33 \times (\text{number of window units})]$ array representing a state transition vector, or how the FNC state changed through time for each subject.

Subsequently, we performed a clustering analysis to examine the structure and frequency of FNC patterns that recurred in the state transition vectors. The k-means clustering algorithm was applied to the individual arrays of FNC covariance matrices using the City method and the algorithm iterated a maximum of 200 times before convergence. We iterated this method to discover the extent to which results were sensitive to variations in the number of clusters selected and the size of the Gaussian window. Based on our prior work (Allen et al., 2014) we chose an initial parameter set of 6 states and a window size of 30TR, and varied parameters around this for a sensitivity analysis including 5, 6 and 7 clusters, each with window sizes of 25, 30 and 35TR (and therefore with 169, 164 and 159 window units respectively) for a total of 9 permutations. In addition, we applied a threshold concept requiring that a given FNC covariance matrix be present in a minimum number of 10 windows for each subject included.

We note that there is an overall structure to the dFNC matrices that appears constant among the clusters and somewhat resembles a 'skeleton' structure of pairwise correlations that recurs from cluster to cluster. This is an expected effect that may also be seen in comparable analyses in other disorders (Rashid et al., 2014) and may reflect the high proportion of variance in brain activity that is thought to remain similar regardless of the task being performed or individual brain state (Cole et al., 2014). In addition, in every permutation there is a matrix in which most networks appear to be correlated. These 'red states' do appear in dynamic connectivity analysis of other, separate datasets and

appear to be clusters representative of the mean of all variance examined. We examined the individual subjects present in this state in the current analysis and they were drawn from all sites, supporting that in this current study this cluster or state may also be the mean. We note that no significant group differences were found in this 'red' state in any of the 9 permutations of the dynamic analysis and therefore it does not influence the direction of our reported results.

2.9. Dynamic connectivity statistical analysis

We computed five measures of dynamic connectivity. Significant group differences in FNC were computed for each state using two-sample t -tests at $\alpha = 0.05$, corrected to control FDR. We also calculated the number of times each subject moved between states during their individual timecourse, the average time (in windows) that each subject spent in each of the states once entering that state (dwell time), and the fraction of their total timecourse each subject spent in each state. Two sample t -tests were performed in these timing measures to examine significant ($\alpha = 0.05$, corrected for dwell and fractional time to control FDR) differences between subjects with autism and healthy controls. Finally, we calculated the number of subjects within each group (controls and subjects affected by autism) present in each state and used two sample t -tests to examine significant ($p < 0.05$) differences between groups in this measure.

2.10. Test-retest reliability analysis

We performed a test-retest analysis on two subsets of the data to ascertain whether the basic directionality of our core results was reliable. Firstly, the dataset was split into group 1 and group 2 of equal size to create two half-size datasets with similar characteristics to each other and the larger group (Supplementary Data Table 4). Prior to statistical testing, we performed a regression between the base FNC 33×33 matrix (Fig. 1) and that of the subgroups to test their similarity. Subsequently, we examined group differences in power spectra, spatial maps, steady-state FNC and dynamic measures (for the median 6 state, 30TR window solution) in the subgroups using the same experimental parameters as in the larger dataset. Since the sub-groups have less power and half the degrees of freedom, we performed steady-state voxelwise statistical t -tests at a significance level of 0.05, with correction for FDR.

3. Results

3.1. A high order model delineated the steady-state connectome at multiple hierarchical levels

We assembled a 33×33 network matrix of interactions in a high order model, representing steady-state FNC across the whole brain for all subjects, including individuals with ASD and controls (Fig. 1a). There were no residual motion effects in FNC with the exception of reduced correlation in the three network pairs of INs 14×22 , 12×29 and 32×33 . In the test-retest analyses, FNC matrices for subgroups 1 and 2 displayed 99.7% and 99.9% correlation with the full group FNC matrix respectively. Spatial maps were grouped according to their neurocognitive function (Fig. 1b), with visual examples of the control network groups displayed (Fig. 1c) here. Among task positive networks, we extracted and positively identified the salience, ventral attention, right and left fronto-parietal, cingulo-opercular, and dorsal attention networks and three default mode networks: core, anterior and posterior. We identified 7 visual, 7 sensorimotor, 4 other control and 6 language networks (Supplementary Fig. 1 and Supplementary Table 4).

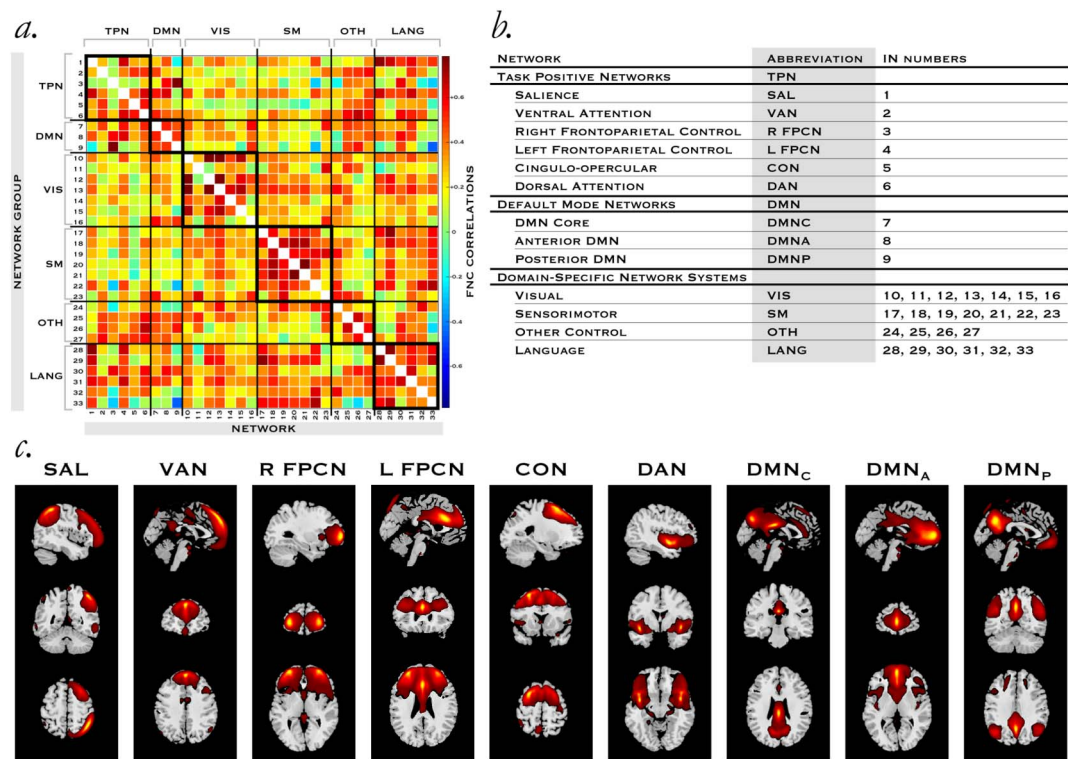


Fig. 1. The steady-state functional connectome in a high order model. **a**, Pearson pairwise correlations between networks averaged across the fMRI timecourses delineate a 33×33 network matrix of interactions in a high order model, representing steady-state FNC across the whole brain for all subjects, including individuals with ASD and controls. We grouped networks by their primary neurocognitive function **b**, into systems. Members of the task positive and default mode control system **c**, are shown in greater detail with slices corresponding to the peak intensity activation in each plane. Coordinates for each network including right and left maxima for the top three regions are available in Supplementary Table 4.

3.2. Bidirectional steady-state control network differences in ASD center on inter-network connectivity

In subjects with ASD, we identified significant differences in inter-network pairwise FNC after controlling for IQ, site, motion, medication status, presence of comorbid diagnoses, eyes open or closed, age and gender (correcting for multiple comparisons at $\alpha = 0.01$ to control FDR). In FNC, we found reduced connectivity strength (hypo-connectivity) between the right fronto-parietal network and both the core and anterior default mode networks, with these effects replicated in both subgroups of the test-retest. Hypo-connectivity was also observed between the ventral attention and left fronto-parietal networks, though this effect was not reliably replicated in either test-retest subgroup. We also detected hypo-connectivity in the anterior-posterior axis of the default mode networks, replicating this effect in subgroup 1. By contrast, the cingulo-opercular network showed abnormally increased correlation (hyper-connectivity) with the anterior DMN, replicated in subgroup 2 in test-retest. This was the only instance of hyper-connectivity we identified in steady-state FNC. There was no interaction of residual motion with FNC group effects in any pair of control networks. We did not find differences between subjects with autism and controls in either measure associated with intra-network integrity (spatial maps and power spectra) in this high order model, and replicated this negative finding in both subgroups in test-retest.

Of the 5 unique network pairings that were disrupted in control networks, DMN sub-networks were involved in 4 of these, including hypo-connectivity in the anterior-posterior DMN axis. Here, our findings parallel much of the extant literature in autism. More specifically, hypo-connectivity among the sub-networks or nodes of the DMN (Assaf et al., 2010; Jung et al., 2014) and anterior-posterior hypo-connectivity in the DMN, (Starck et al., 2013) have been highlighted as the best-replicated findings in the (albeit heterogeneous) autism connectivity literature (See review by Hull et al (Hull et al., 2016)).

In task-positive networks, it is more challenging to compare our results with others due to fewer studies, and methodologic and subject selection differences. For example, in 40 children with ASD, Abbott et al. identified hyper-connectivity between the DMN and executive (fronto-parietal) control network, in contrast to our finding of hypo-connectivity, though this study examined 4 networks in a lower model order, treating the fronto-parietal network as a single entity (Abbott et al., 2016). We identified a locus of hyper-connectivity involving the cingulo-opercular network, where the insula is one of two core regions. The insula and its connections have recently acquired more prominence in the autism, but it is also a core constituent of the salience network. These networks somewhat overlap (Power et al., 2011), as may be seen in Fig. 1c, and ideally, both networks would be present in any one model to allow effective inter-study comparisons: most extant studies focus on one or the other network. Connectivity differences in the insula and salience networks have been well-demonstrated in autism, particularly in multiple interesting studies by the Uddin group (Uddin et al., 2013; Uddin and Menon, 2009). With respect to the cingulo-opercular network, Chen et al. (Chen et al., 2016) found disrupted connectivity among the cingulo-opercular, fronto-parietal networks and DMN and intriguingly, Nomi & Uddin detected a ‘weaker functional relationship between the DMN and a [non-salience] subcortical/insula component’ in adolescents with ASD (Nomi and Uddin, 2015). Our finding of hyper-connectivity between cingulo-opercular and anterior DMN differs from this general trend of identifying hypo-connectivity in insula-related networks. In this regard, more studies in autism including both salience and cingulo-opercular networks will be helpful to disambiguate effects. In terms of the canonical DMN-dorsal attention circuit, our finding that this had normal connectivity parallels work by others (Nomi and Uddin, 2015; Kennedy and Courchesne, 2008).

Our negative results in measures of intra-network disruption in control networks are in accordance with some studies (Abbott et al., 2016; Bos et al., 2014), but other groups have detected differences in

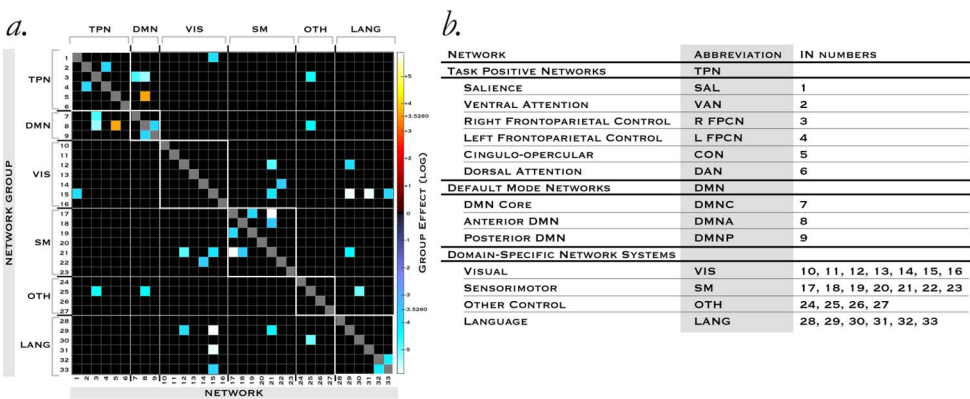


Fig. 2. Steady-state FNC differences in ASD. a, Significant differences (log scale) in functional connectivity measures between b, pairs of networks after controlling for IQ, site, motion, age, gender, eyes open/closed, medication and co-morbidity status, corrected for multiple comparisons at $\alpha = 0.01$ to control false discovery rate (FDR).

intra-network measures, and an important school of thought exists conceptualizing ASD as a disorder where local hyper-connectivity contrasts with long-range hypo-connectivity (Geschwind and Levitt, 2007). Fewer studies specifically focusing on TPN networks as distinct from the DMN exist, and age stratification, may also be an important influence in detecting these effects on a network basis. For example, Farrant & Uddin (Farrant and Uddin, 2016) detected hyper-connectivity within the dorsal and ventral attention networks in children with ASD, but hypo-connectivity in adults. Model order is also worthy of consideration, since intra-network disruption in a low model order might appear as inter-network disruption among sub-networks in a higher model order.

3.3. Domain networks showed pervasive reduced inter-network connectivity in ASD

Control networks exert configurative influence over downstream domain-specific networks. We also identified group effects in domain-specific networks. Sensory abnormalities are common in ASD, encompassing visual, tactile, auditory and olfactory processing differences, with a common theme of atypical perceptual integration. Motor features - predominantly stereotypies, sometimes called ‘stimming’ - have been of particular interest as possible diagnostic markers since they precede communication deficits at ages 6–12 months. Paralleling our findings in control networks, we identified widespread differences in pairwise FNC in domain networks in ASD (Fig. 2), but not in spectra or spatial maps, again suggesting that disruption is centered on the functional relationships between networks rather than their intra-network integrity. However, a contrasting finding was that in domain networks the direction of these pairwise differences was uniformly of reduced correlation strength. A total of 16 unique pairwise differences were detected in domain-specific networks in autism. We observed reduced correlation in three network pairs of INs 14×22 , 12×29 and 32×33 where we had detected possible motion contamination rendering these group effects potentially spurious, and we therefore discounted them in reporting results. Of the remaining 13, every group effect except IN17x19 (two sensorimotor networks) was present IN at least one of the test-retest subgroups, with three pairs (12×21 , 17×21 and 15×31) appearing in both.

Language impairment exhibits great inter-individual variability in ASD. We found disruption to FNC in 4 language networks in 7 pairwise network relationships. Interestingly, three of these were with a single higher-level visual processing network (IN15). Three visual networks displayed pairwise reduced connectivity strength in 8 pairings, including both lower-level (IN 12 and 14) and higher-level (IN 15) visual processing networks. Well-known visual perceptual differences in ASD are characterized by deficits in global processing (whole object) but superior low level processing (object details), and recent causative explanations have focused on a lack of integration between low- and high-level visual processes (Smith et al., 2015). In sensorimotor networks,

we identified FNC differences in 5 networks in 10 pairings, most commonly with visual or other sensorimotor networks. IN21, the right primary sensorimotor network, displayed the most frequent deficits, with hypo-connectivity in four pairwise relationships. Two of these, with IN12 (a visual network) and IN17 (a sensorimotor network) replicated in both subgroups in test-retest. These prominent effects in the primary right sensorimotor network are noteworthy given motor stereotypies are a cardinal feature of ASD.

3.4. Group effects in FNC in control and domain-specific networks were unaffected by IQ level

Intellectual disability is a significant co-morbidity with ASD. In contrast to most published studies using large datasets, we included subjects with co-morbid intellectual disability and low normal IQ (< 80). IQs ranged from 41 to 148 (mean = 108) and were normally distributed in our subject group, with 27% below the population mean of 100. Importantly, no FNC effects were attributable to IQ or an IQ x autism interaction (replicated in test-retest), indicating that ASD may have an FNC phenotype that is independently detectable. While significant FNC effects were attributable to age (though not an age x autism interaction), this is consistent with results in unaffected individuals (Allen et al., 2011), reflecting a generalized maturation process.

3.5. System-based measures demonstrated a mix of hyper- and hypo-connectivity

To complement intra-network and inter-network measures we examined connectivity relationships in groups of networks, arranged by their neurocognitive function (Supplementary Fig. 1). In autism (Fig. 3), we identified significantly decreased within-system connection strength in the default mode network group (comprising the three DMN subnetworks) and the group of other control networks. Since this is a high order model which decomposes the DMN into constituent sub-networks, this finding may be conceptually related to findings by others of disruption within the DMN in lower order models, as discussed above. By contrast, we identified abnormally increased connectivity within the visual network group. There was no difference between autism and controls in the intra-system measure in the TPN, sensorimotor or language groups. When relationships between systems of networks was considered, there was also a mix of hyper- and hypo-connectivity, though as with individual FNC, hypo-connectivity predominated. Reduced inter-system connection strength most affected the visual system, in its connections to language, sensorimotor and TPN systems, and the TPN group relationship to other control networks. However, we observed hyper-correlation between the language and DMN systems.

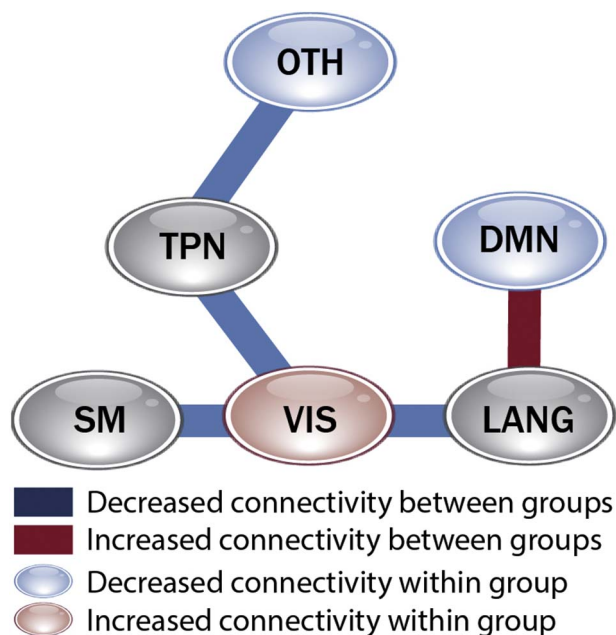


Fig. 3. Intra-system and inter-system connectivity in ASD.

Group effects in correlations between networks within a neurocognitive system (bubbles), and between systems (lines) corrected at $\alpha = 0.05$ to control FDR.

3.6. Dynamic connectivity analysis delineates a temporal structure of dysconnectivity in ASD

Most fMRI connectivity analyses use steady-state measures, aggregating averaged connections to create a summative, stationary picture of whole-brain network configuration. However, functional connectivity and FNC are non-stationary, exhibiting dynamic shifts that also display spatiotemporally patterned organization. Sustained temporal synchrony among networks creates multiple separable, persistent states observable in fMRI (Calhoun et al., 2014; Cole et al., 2013). States likely instantiate the multi-scale spatio-temporal organization of information processing, enabling transitions between processing modes

(e.g. attentional shifts) and the application of established templates to novel tasks and consolidation of learning. As patterns of intra-network regional coupling facilitate the formation of task-specific templates at a lower hierarchical level, these dynamic configuration templates may frame efficient inter-network brain state transitions and represent a “latent functional architecture” enabling higher cognition (Spreng et al., 2013). Newer dynamic FNC techniques using fMRI can delineate variability in FNC over the resting state neuroimaging time-course and have become a powerful new tool to elucidate the mechanisms of state changes underlying behavior and cognition (Calhoun et al., 2014) successfully discriminating patient groups in schizophrenia and bipolar disorders (Rashid et al., 2014). To date, these concepts have only been applied in ASD to data from a handful of brain regions in small samples (Falahpour et al., 2016) and have not been performed on a whole brain, network basis.

Unlike conventional FNC analysis that averages across the rsfMRI timecourses, this dynamic approach can separate significant differences in patterns of abnormal connectivity and locate these in individual states, providing a more granular picture of the structure of functional connectivity in ASD. Here, the 6 state, 30TR-size window solution is displayed (Fig. 4), with the full set of state transition matrices for control subjects in the sensitivity analysis available for comparing the effects of parameter variation (Supplementary Fig. 3).

Analysis of group effects (‘Difference’) shows significant (corrected for multiple comparisons at $\alpha = 0.05$ to control FDR) pairwise differences in multiple states. As in steady-state FNC, a mix of abnormally decreased and increased correlation is evident in control network pairings with decreased connectivity more common among domain-specific networks. While research is still at too early a stage to attribute specific behaviors or tasks that may be associated with individual brain states identified in dynamic resting-state analysis, we note that disruption to the overall configuration of pairwise correlations is most common in certain states. In these states there is more diffuse anticorrelation, particularly in the relationships among network systems vs within systems, and between the control network vs sensorimotor and visual groups. In particular, the right fronto-parietal control network is anticorrelated with most other TPN members.

We compared results across the sensitivity analysis (Fig. 5) and were particularly interested in group differences present regardless of the

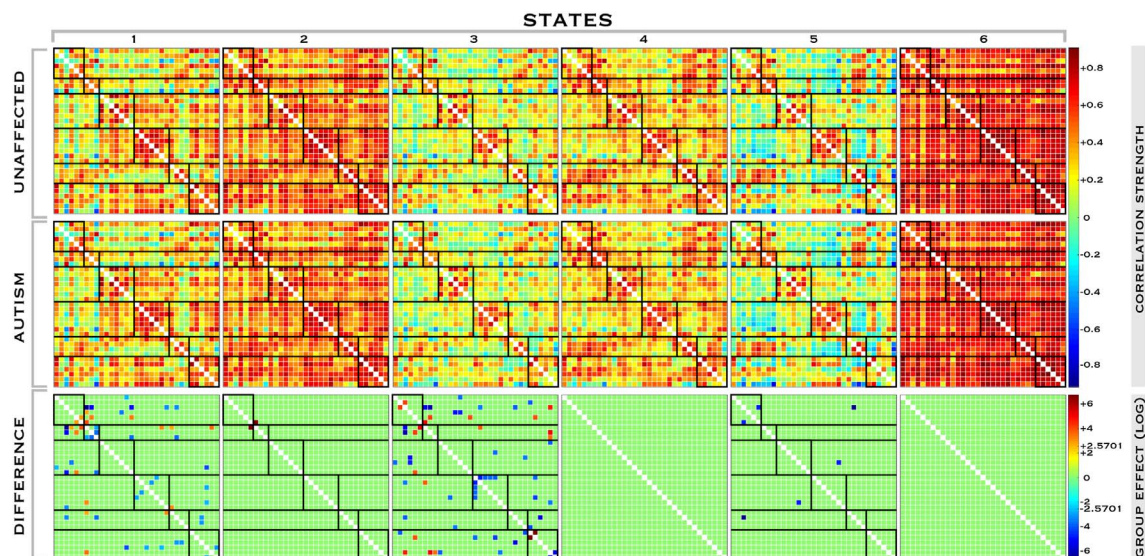


Fig. 4. Dynamic functional connectivity across brain states in controls and subjects with ASD.

Distinct, stable brain states exist within the aggregated resting state timecourses each with a specific FNC pattern. Each 33×33 network matrix is composed of Pearson pairwise correlations (color scale) between the 33 networks identified in the group independent component analysis for all subjects, decomposed into individual states using k-means clustering. We computed 9 permutations of this analysis with the 6 state, 30TR-size window solution shown here. Dynamic connectivity in control subjects (‘Unaffected’) is compared to that in individuals with ASD (‘Autism’) and significant group effects (‘Difference’) displayed for each individual state (log scale). Significant pairwise differences in FNC for each state are displayed, corrected for multiple comparisons at $\alpha = 0.05$ to control FDR.

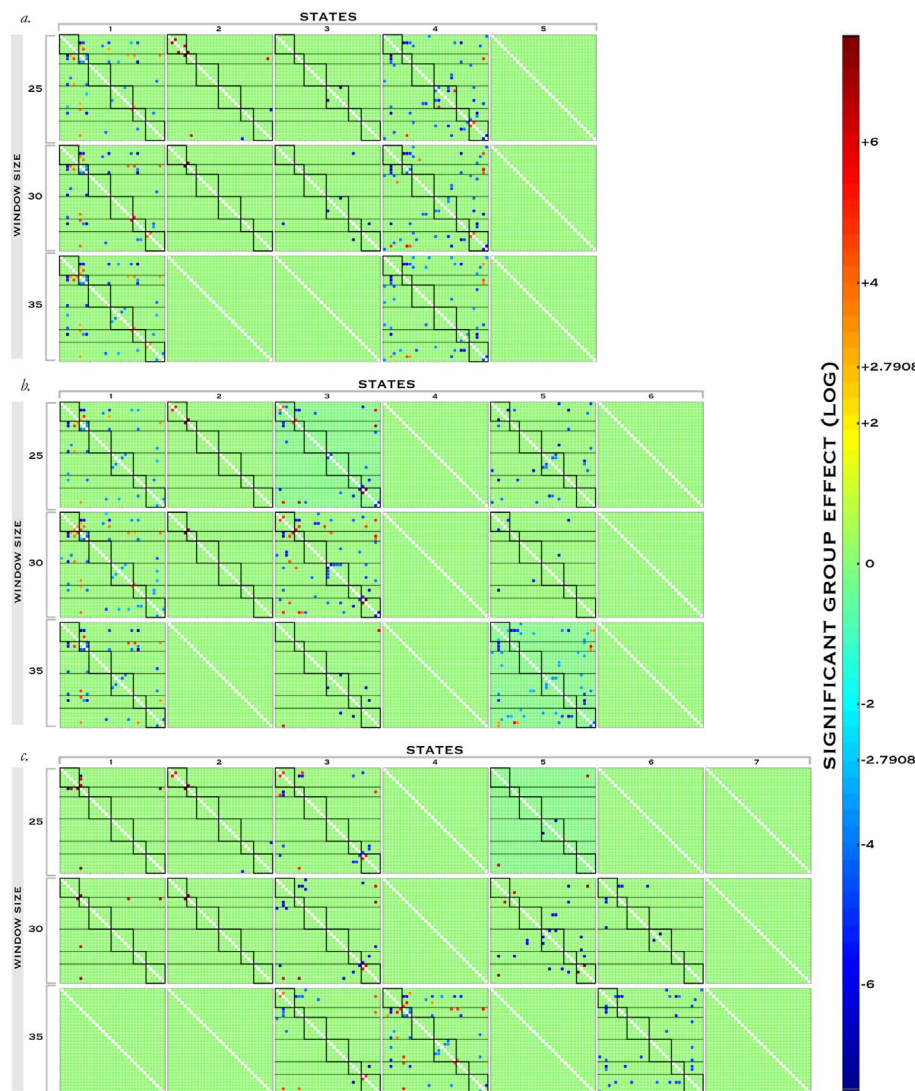


Fig. 5. Group Differences in Dynamic Connectivity Sensitivity Analysis.

Group differences in autism vs controls for each permutation of the dFNC analysis. Significant pairwise differences in FNC for each state are displayed, corrected for multiple comparisons at $\alpha = 0.05$ to control FDR.

window size, and observable in ≥ 2 state number variants. Among control networks, hypo-correlation between the right fronto-parietal network and core DMN, in the anterior and posterior DMN axis, and hyper-correlation between the cingulo-opercular network and anterior DMN met these criteria. These were also robust in steady-state FNC and replicated in 1 + sub-group in dFNC test-retest. Hypo-correlation of the right fronto-parietal control network with the anterior DMN was the single most robust finding in our entire pipeline, present in all 9 dFNC permutations, sub-group 1 of the dFNC test-retest, the steady-state analysis and both steady-state test-rest groups. However, hypocorrelation between the ventral attention and left fronto-parietal networks seen in steady-state did not meet these criteria or replicate in dFNC test-retest. Two other connections that were not present in the steady-state analysis were robust to parameter variation in the dFNC sensitivity, namely hypoconnectivity between the posterior DMN and both the right fronto-parietal network and core DMN, but were not replicated in the dFNC test-retest analysis.

Domain network group effects in dFNC were less consistent between steady-state and dynamic FNC, and within permutations of the dFNC sensitivity analysis, showing particular paucity in the 7 state solution. Despite the greater numbers of domain-specific networks, only three group differences were as robust as the highlighted control networks effects across the dFNC sensitivity analysis. Two of these observations involved language networks, and were between INs 25 and 30 (present in all 9 permutations, and in sub-group 2 in the test-retest) and INs 32

and 8 (present in two states and all windows, but not test-retest), though these effects were not present in the steady-state FNC. However, the third was a connectivity deficit (appearing in 2 states and all window variants) between the right primary sensorimotor network and a high-level visual network (IN21x17) that replicated strongly in the steady-state FNC analysis, though not in the dFNC test-retest.

3.7. The tempo of brain state transitions may be jittered in ASD

The disruption we identified in the fronto-parietal networks implies alteration to start-cues, while that in the cingulo-opercular network suggests impaired state maintenance. Therefore, we predicted loss of appropriate tempo in brain state transitions in ASD. Our results suggest disrupted state transition tempo does exist in ASD in the form of a significant decrease in the number of times subjects with autism change brain state. This result varied somewhat across permutations of the dFNC analysis, but oscillations were significantly dampened in autism in 5/9 permutations, and narrowly missed significance in 4 more, making it a fairly robust finding (Fig. 6) in the sensitivity analysis, though it did not replicate in test-retest. We did not detect significant group differences in subjects' dwell time or the fraction of time they spent each state in nearly every permutation of the analysis, with scattered exceptions. Differences in the number of subjects in each state was never significant.

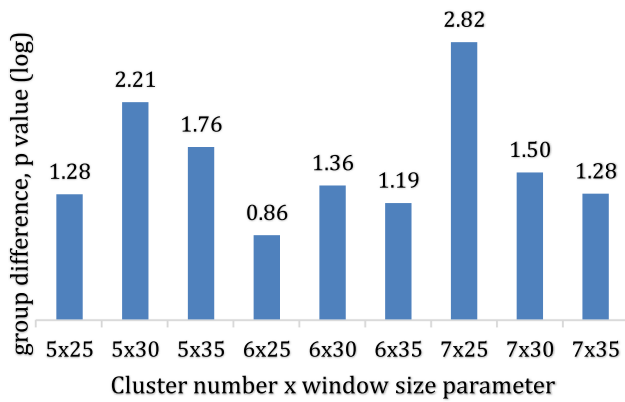


Fig. 6. Difference in the number of times subjects changed states in ASD. For each permutation of the dynamic connectivity analysis (horizontal axis), the significance of the group difference is shown, where $p_{\log_{10}} = 1.30$ is equivalent to $p = 0.05$. The number of times subjects changed states was significant or almost significant in every permutation except the 6 state, 25TR solution.

4. Discussion

During the first year of life the simple IN architecture present at birth reorganizes in a sequenced trajectory supporting brain functional maturation. The cingulo-opercular network differentiates out of the fronto-parietal control networks, DMNs proliferate, sensorimotor, visual and attention networks reorganize and overall long-range connectivity increases (Fair et al., 2007). Control networks operate at the highest logical level of brain organization, exerting downstream configurative effects.

The control system backbone comprises sets of specific task-positive (TPN) and default mode networks (DMN, Fig. 1) (Cole et al., 2013). The Petersen-Posner attention model proposes that the dorsal attention network selects sensory stimuli based on internal goals/expectations (orienting) while the ventral attention network is activated by behaviorally important but unexpected stimuli (reorienting), and controls recovery from attentional lapses. Reorienting enables the improvisation of novel, task-relevant actions and adaptive function. Executive control incorporates and extends this basic attentional scaffold (Petersen and Posner, 2012). In the influential dual network view of executive control, the fronto-parietal control networks and certain ventral attention regions (Dosenbach et al., 2006) provide transient start cue signals before a task-specific spatio-temporal FNC configuration is instantiated to perform a task. The cingulo-opercular network follows with a sustained task-general maintenance signal (Dosenbach et al., 2007; Sestieri et al., 2014) to keep the brain online. Core cingulo-opercular (dorsal anterior cingulate, bilateral insula) and more anterior fronto-parietal control network regions also perform error/performance feedback (Dosenbach et al., 2006; Dosenbach et al., 2007) with a salience network believed to maintain alertness and visual attention (Sadaghiani et al., 2010). Early work in fMRI (Fox et al., 2009) identified a reciprocal anticorrelated relationship between the dorsal attention network and correlated regions named the default mode network that became deactivated when the brain entered 'task-positive' mode and vice versa. This default mode network was accordingly associated with 'task-negative' and introspective modes of brain function. Extending this, three default mode subsystems have recently been identified: Anterior (DMN_A) involved in emotion inhibition, goal-directed and social cognition, posterior (DMN_P) in memory, self-reflection and autobiographical conceptualization, and core (DMN_C) that may facilitate intra-DMN information transfer (Andrews-Hanna et al., 2014). The combined TPN-DMN system is now understood to implement executive control by shifting the spatio-temporal patterning of whole-brain FNC states (Cole et al., 2013; Uddin et al., 2009) to implement specific or integrative tasks. Downstream, domain networks respond by

reconfiguring their activation patterns (Dosenbach et al., 2007). Characterizing a detailed model of whole brain FNC incorporating control network relationships represents a substantial technical challenge in fMRI data. Specifically, a high order model of > 20 networks is required, since low order models fail to divide the lateralized fronto-parietal control networks (Smith et al., 2009), disambiguate the spatially overlapping cingulo-opercular from salience networks (Power et al., 2011) and separate the DMN subsystems (Andrews-Hanna et al., 2014).

In subjects with ASD, our work demonstrates disruption in the control networks that are vulnerable to altered differentiation during the infant period, and traces the sequelae that propagate dynamically through the chronnectomic hierarchy. The correspondence between our findings, events in the normal developmental sequence of networks during infancy, and the unique infantile age of onset of ASD suggests that early disrupted network maturation from diverse causes may manifest as a convergent macroscale functional phenotype in ASD. Our results suggest substantial differences in the function of certain control networks in autism, particularly those associated with task cues and task maintenance, and the 'task-negative' default mode networks, comporting with conceptualizations of autism as being in part a 'disorder of control' (Fair et al., 2007). These results in the resting-state suggest alterations to the networks that support executive/top-down processes operating in the brain to control the instantiation, maintenance and switching of the functional connectivity configurations that subserve tasks. Thus, they led us to predict that there would be alteration to dynamic states, where we identified disrupted dynamic FNC configurations, and a dampening to subject oscillations among brain states. Since these findings are in imaging obtained in the resting-state, and connectivity configurations in this condition are hypothesized to be templates that are active in task-performance, it raises the important question of whether our findings could be demonstrated in task conditions in autism.

Our model consistently confirmed the importance of abnormalities in control network architecture in ASD, and of the central role of inter-network connectivity, in both steady-state and dynamic measures. We provide an integrated, detailed picture of whole-brain connectivity in autism that proposes certain motifs may operate across this heterogeneous disorder, notwithstanding the variability among individuals in terms of neurocognitive findings, IQ level and psychiatric comorbidities. This coherent framework may help reconcile disparate previous observations (such as debates regarding short- versus long-range or under- versus over-connectivity), elucidate connectivity patterns that have hitherto been obscure, and demonstrate that not only the spatial but also the temporal organization of brain function is disturbed in ASD. We found that control networks as a group exhibit proportionally more deficits that are consistent between steady-state and dynamic FNC measures than domain-specific networks. This observation may be autism-specific, or may be attributable to control networks having more inherent variability in their correlations across brain states, and warrants further investigation.

Our aim in this study was to bring together many outcome measures spanning steady-state and dynamic connectivity to compare findings across these techniques in a high-order model and large, varied subject group. When we consider results from this perspective, guided also by our findings in sensitivity and test-retest analysis, several specific network connections are prominent. Deficits in the right fronto-parietal-DMN_A, right fronto-parietal-DMN_C, and cingulo-opercular-DMN_A circuits, and in the DMN_A-DMN_P axis proved quite robust (Fig. 7), and may link mechanistically to the disrupted state change tempo that we identified in autism. Further investigation of these motifs, for example by exploring their presence in sub-populations of ASD, other conditions such as task-based fMRI, and comparisons to other developmental neuropsychiatric disorders, would help confirm their specificity and potential to elucidate mechanisms of ASD behaviors.

The collection of resting state fMRI data is not confounded by

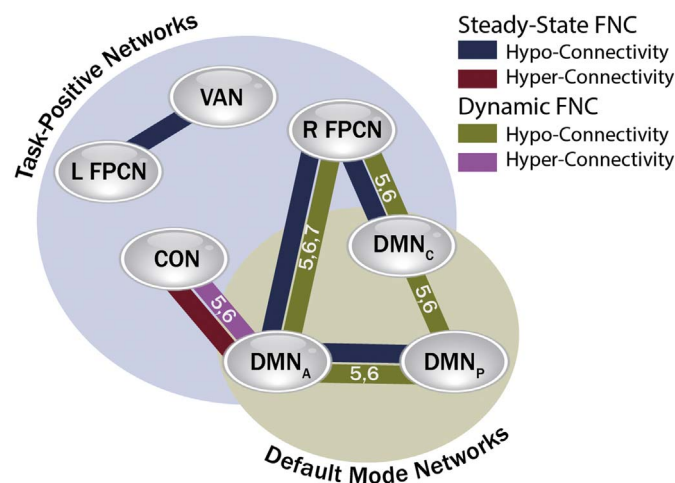


Fig. 7. The control network chronnectome in ASD.

A web of abnormal functional connectivity affecting brain control networks is centered on the right fronto-parietal control network and default mode network in autism. We superimpose pairwise disruption visible in the steady-state and dynamic connectomes (with the specific dynamic state in which dFNC findings appear noted as a number within the line connection) to illustrate the importance of analyzing dynamic connectivity in building an integrated understanding of the differences in connectivity in this complex neuropsychiatric disorder.

behavioral, motor or language performance requirements and is highly efficient, with 6 min of data sufficient to reliably capture networks and provide multiple outcome measures (Allen et al., 2011). Network connectivity measures obtained from resting state fMRI hold great promise to further inform our understanding of human brain development and function and provide neuropsychiatric biomarkers and treatment targets for disorders such as ASD. Future studies comparing conditions distinct from and overlapping with ASD will inform the specificity of these findings.

5. Author contributions

N.dL conceived the study design, and performed data preparation, neuroimaging and statistical analysis with input from V.D.C.; V.D.C conceived the study design and developed the methods and software used in the analysis; D.D. and B.H.K. participated in study design. S.R. performed algorithm development and coding. N.dL wrote the manuscript with input from V.D.C, D.D. and B.H.K.

Supplementary data to this article can be found online at <http://dx.doi.org/10.1016/j.nicl.2017.05.024>.

Acknowledgements

The authors thank Cameron Craddock and Chao-Gan Yan from The Child Mind Institute for their clarification of collection methods in the ABIDE dataset. We also thank Brian A. Dickinson for his assistance with coding, suggestions and proofreading, and B. Ernesto Johnson for his assistance with pairwise correlation mapping and figure preparation. This work was supported by the American Psychiatric Institute Janssen Scholar Award, and the National Center For Advancing Translational Sciences of the National Institutes of Health under Award Number UL1TR000423 to N.d.L and by the National Institutes of Health under grants P20GM103472 and R01EB020407 and the National Science Foundation under award 1539067 to V.D.C. The content is solely the responsibility of the authors and does not necessarily represent the official views of the National Institutes of Health. The authors declare they have no conflicts of interest.

References

- Abbott, A.E., et al., 2016. Patterns of atypical functional connectivity and behavioral links in autism differ between default, salience, and executive networks. *Cereb. Cortex* 26, 4034–4045. <http://dx.doi.org/10.1093/cercor/bhv191>.
- Allen, E.A., et al., 2011. A baseline for the multivariate comparison of resting-state networks. *Front. Syst. Neurosci.* 5, 2. <http://dx.doi.org/10.3389/fnsys.2011.00002>.
- Allen, E.A., Erhardt, E.B., Wei, Y., Eichele, T., Calhoun, V.D., 2012. Capturing intersubject variability with group independent component analysis of fMRI data: a simulation study. *NeuroImage* 59, 4141–4159. <http://dx.doi.org/10.1016/j.neuroimage.2011.10.010>.
- Allen, E.A., et al., 2014. Tracking whole-brain connectivity dynamics in the resting state. *Cereb. Cortex* 24, 663–676. <http://dx.doi.org/10.1093/cercor/bhs352>.
- Andrews-Hanna, J.R., Smallwood, J., Spreng, R.N., 2014. The default network and self-generated thought: component processes, dynamic control, and clinical relevance. *Ann. N. Y. Acad. Sci.* 1316, 29–52. <http://dx.doi.org/10.1111/nyas.12360>.
- Anticevic, A., et al., 2014. Global resting-state functional magnetic resonance imaging analysis identifies frontal cortex, striatal, and cerebellar dysconnectivity in obsessive-compulsive disorder. *Biol. Psychiatry* 75, 595–605. <http://dx.doi.org/10.1016/j.biopsych.2013.10.021>.
- Assaf, M., et al., 2010. Abnormal functional connectivity of default mode sub-networks in autism spectrum disorder patients. *NeuroImage* 53, 247–256. <http://dx.doi.org/10.1016/j.neuroimage.2010.05.067>.
- Bokil, H., Andrews, P., Kulkarni, J.E., Mehta, S., Mitra, P.P., 2010. Chronux: a platform for analyzing neural signals. *J. Neurosci. Methods* 192, 146–151. <http://dx.doi.org/10.1016/j.jneumeth.2010.06.020>.
- Bos, D.J., et al., 2014. Developmental differences in higher-order resting-state networks in autism spectrum disorder. *NeuroImage Clin* 4, 820–827. <http://dx.doi.org/10.1016/j.nicl.2014.05.007>.
- Buescher, A.V., Cidav, Z., Knapp, M., Mandell, D.S., 2014. Costs of autism spectrum disorders in the United Kingdom and the United States. *JAMA Pediatr.* 168, 721–728. <http://dx.doi.org/10.1001/JAMAPEDIATRICS.2014.210>.
- Calhoun, V.D., Adali, T., 2012. Multisubject independent component analysis of fMRI: a decade of intrinsic networks, default mode, and neurodiagnostic discovery. *IEEE Rev. Biomed. Eng.* 5, 60–73. <http://dx.doi.org/10.1109/RBME.2012.2211076>.
- Calhoun, V.D., Miller, R., Pearlson, G., Adali, T., 2014. The chronnectome: time-varying connectivity networks as the next frontier in fMRI data discovery. *Neuron* 84, 262–274. <http://dx.doi.org/10.1016/j.neuron.2014.10.015>.
- Chen, H., et al., 2016. Multivariate classification of autism spectrum disorder using frequency-specific resting-state functional connectivity—a multi-center study. *Prog. Neuro-Psychopharmacol. Biol. Psychiatry* 64, 1–9. <http://dx.doi.org/10.1016/j.pnpb.2015.06.014>.
- Cole, M.W., et al., 2013. Multi-task connectivity reveals flexible hubs for adaptive task control. *Nat. Neurosci.* 16, 1348–1355. <http://dx.doi.org/10.1038/nn.3470>.
- Cole, M.W., Bassett, D.S., Power, J.D., Braver, T.S., Petersen, S.E., 2014. Intrinsic and task-evoked network architectures of the human brain. *Neuron* 83, 238–251. <http://dx.doi.org/10.1016/j.neuron.2014.05.014>.
- Di Martino, A., et al., 2014. The autism brain imaging data exchange: towards a large-scale evaluation of the intrinsic brain architecture in autism. *Mol. Psychiatry* 19, 659–667. <http://dx.doi.org/10.1038/mp.2013.78>.
- Dosenbach, N.U., et al., 2006. A core system for the implementation of task sets. *Neuron* 50, 799–812. <http://dx.doi.org/10.1016/j.neuron.2006.04.031>.
- Dosenbach, N.U., et al., 2007. Distinct brain networks for adaptive and stable task control in humans. *Proc. Natl. Acad. Sci. U. S. A.* 104, 11073–11078. <http://dx.doi.org/10.1073/pnas.0704320104>.
- Du, Y., et al., 2015. A group ICA based framework for evaluating resting fMRI markers when disease categories are unclear: application to schizophrenia, bipolar, and schizoaffective disorders. *NeuroImage* 122, 272–280. <http://dx.doi.org/10.1016/j.neuroimage.2015.07.054>.
- Duerden, E.G., Mak-Fan, K.M., Taylor, M.J., Roberts, S.W., 2012. Regional differences in grey and white matter in children and adults with autism spectrum disorders: an activation likelihood estimate (ALE) meta-analysis. *Autism research : official journal of the International Society for Autism Research* 5, 49–66. <http://dx.doi.org/10.1002/aur.235>.
- Eklund, A., Nichols, T.E., Knutsson, H., 2016. Cluster failure: why fMRI inferences for spatial extent have inflated false-positive rates. *Proc. Natl. Acad. Sci. U. S. A.* 113, 7900–7905. <http://dx.doi.org/10.1073/pnas.1602413113>.
- Erhardt, E.B., et al., 2011. Comparison of multi-subject ICA methods for analysis of fMRI data. *Hum. Brain Mapp.* 32, 2075–2095. <http://dx.doi.org/10.1002/hbm.21170>.
- Fair, D.A., et al., 2007. Development of distinct control networks through segregation and integration. *Proc. Natl. Acad. Sci. U. S. A.* 104, 13507–13512. <http://dx.doi.org/10.1073/pnas.0705843104>.
- Falahpour, M., et al., 2016. 'Underconnected', but not broken? Dynamic fMRI shows underconnectivity in autism is linked to increased intra-individual variability across time. *Brain Connectivity*. <http://dx.doi.org/10.1089/brain.2015.0389>.
- Farrant, K., Uddin, L.Q., 2016. Atypical developmental of dorsal and ventral attention networks in autism. *Dev. Sci.* 19, 550–563. <http://dx.doi.org/10.1111/desc.12359>.
- Fox, M.D., et al., 2005. The human brain is intrinsically organized into dynamic, anticorrelated functional networks. *Proc. Natl. Acad. Sci. U. S. A.* 102, 9673–9678. <http://dx.doi.org/10.1073/pnas.0504136102>.
- Fox, M.D., Zhang, D., Snyder, A.Z., Raichle, M.E., 2009. The global signal and observed anticorrelated resting state brain networks. *J. Neurophysiol.* 101, 3270–3283. <http://dx.doi.org/10.1152/jn.90777.2008>.
- Geschwind, D.H., Levitt, P., 2007. Autism spectrum disorders: developmental disconnection syndromes. *Curr. Opin. Neurobiol.* 17, 103–111. <http://dx.doi.org/10.1016/j.con.2007.05.001>.

- 1016/j.conb.2007.01.009.
- Geschwind, D.H., State, M.W., 2015. Gene Hunting in Autism Spectrum Disorder: on the Path to Precision Medicine. *The Lancet, Neurology*. [http://dx.doi.org/10.1016/S1474-4422\(15\)00044-7](http://dx.doi.org/10.1016/S1474-4422(15)00044-7).
- Herbert, M.R., 2010. Contributions of the environment and environmentally vulnerable physiology to autism spectrum disorders. *Curr. Opin. Neurol.* 23, 103–110. <http://dx.doi.org/10.1097/WCO.0b013e328336a01f>.
- Himberg, J., Hyvarinen, A., Esposito, F., 2004. Validating the independent components of neuroimaging time series via clustering and visualization. *NeuroImage* 22, 1214–1222. <http://dx.doi.org/10.1016/j.neuroimage.2004.03.027>.
- Hull, J.V., Jakobs, Z.J., Torgerson, C.M., Irimia, A., Van Horn, J.D., 2016. Resting-state functional connectivity in autism spectrum disorders: a review. *Front Psychiatry* 7, 205. <http://dx.doi.org/10.3389/fpsy.2016.00205>.
- Hutsler, J.J., Casanova, M.F., 2015. Cortical construction in autism spectrum disorder: columns, connectivity and the Subplate. *Neuropathol. Appl. Neurobiol.* <http://dx.doi.org/10.1111/nan.12227>.
- Jung, M., et al., 2014. Default mode network in young male adults with autism spectrum disorder: relationship with autism spectrum traits. *Mol Autism* 5, 35. <http://dx.doi.org/10.1186/2040-2392-5-35>.
- Kennedy, D.P., Courchesne, E., 2008. The intrinsic functional organization of the brain is altered in autism. *NeuroImage* 39, 1877–1885. <http://dx.doi.org/10.1016/j.neuroimage.2007.10.052>.
- Lai, M.C., Lombardo, M.V., Baron-Cohen, S., 2014. Autism. *Lancet* 383, 896–910. [http://dx.doi.org/10.1016/S0140-6736\(13\)61539-1](http://dx.doi.org/10.1016/S0140-6736(13)61539-1).
- Laird, A.R., et al., 2011. Behavioral interpretations of intrinsic connectivity networks. *J. Cogn. Neurosci.* 23, 4022–4037. http://dx.doi.org/10.1162/jocn_a.00077.
- Li, Y.O., Adali, T., Calhoun, V.D., 2007. Estimating the number of independent components for functional magnetic resonance imaging data. *Hum. Brain Mapp.* 28, 1251–1266. <http://dx.doi.org/10.1002/hbm.20359>.
- Ma, S., et al., 2011. Automatic identification of functional clusters in fMRI data using spatial dependence. *IEEE Trans. Biomed. Eng.* 58, 3406–3417. <http://dx.doi.org/10.1109/TBME.2011.2167149>.
- Manoliu, A., et al., 2013. Insular dysfunction within the salience network is associated with severity of symptoms and aberrant inter-network connectivity in major depressive disorder. *Front. Hum. Neurosci.* 7, 930. <http://dx.doi.org/10.3389/fnhum.2013.00930>.
- Nomi, J.S., Uddin, L.Q., 2015. Developmental changes in large-scale network connectivity in autism. *Neuroimage Clin* 7, 732–741. <http://dx.doi.org/10.1016/j.nicl.2015.02.024>.
- Petersen, S.E., Posner, M.I., 2012. The attention system of the human brain: 20 years after. *Annu. Rev. Neurosci.* 35, 73–89. <http://dx.doi.org/10.1146/annurev-neuro-062111-150525>.
- Power, J.D., et al., 2011. Functional network organization of the human brain. *Neuron* 72, 665–678. <http://dx.doi.org/10.1016/j.neuron.2011.09.006>.
- Rashid, B., Damaraju, E., Pearson, G.D., Calhoun, V.D., 2014. Dynamic connectivity states estimated from resting fMRI identify differences among schizophrenia, bipolar disorder, and healthy control subjects. *Front. Hum. Neurosci.* 8, 897. <http://dx.doi.org/10.3389/fnhum.2014.00897>.
- Sadaghiani, S., et al., 2010. Intrinsic connectivity networks, alpha oscillations, and tonic alertness: a simultaneous electroencephalography/functional magnetic resonance imaging study. *J. Neurosci.* 30, 10243–10250. <http://dx.doi.org/10.1523/JNEUROSCI.1004-10.2010>.
- Seeley, W.W., et al., 2007. Dissociable intrinsic connectivity networks for salience processing and executive control. *J. Neurosci.* 27, 2349–2356. <http://dx.doi.org/10.1523/JNEUROSCI.5587-06.2007>.
- Sestieri, C., Corbetta, M., Spadone, S., Romani, G.L., Shulman, G.L., 2014. Domain-general signals in the cingulo-opercular network for visuospatial attention and episodic memory. *J. Cogn. Neurosci.* 26, 551–568. http://dx.doi.org/10.1162/jocn_a.00504.
- Silver, W.G., Rapin, I., 2012. Neurobiological basis of autism. *Pediatr. Clin. N. Am.* 59, 45–61. <http://dx.doi.org/10.1016/j.pcl.2011.10.010>.
- Smith, S.M., et al., 2009. Correspondence of the brain's functional architecture during activation and rest. *Proc. Natl. Acad. Sci. U. S. A.* 106, 13040–13045. <http://dx.doi.org/10.1073/pnas.0905267106>.
- Smith, D., Ropar, D., Allen, H.A., 2015. Visual integration in autism. *Front. Hum. Neurosci.* 9, 387. <http://dx.doi.org/10.3389/fnhum.2015.00387>.
- Spreng, R.N., Sepulcre, J., Turner, G.R., Stevens, W.D., Schacter, D.L., 2013. Intrinsic architecture underlying the relations among the default, dorsal attention, and frontoparietal control networks of the human brain. *J. Cogn. Neurosci.* 25, 74–86. http://dx.doi.org/10.1162/jocn_a.00281.
- Starck, T., et al., 2013. Resting state fMRI reveals a default mode dissociation between retrosplenial and medial prefrontal subnetworks in ASD despite motion scrubbing. *Front. Hum. Neurosci.* 7, 802. <http://dx.doi.org/10.3389/fnhum.2013.00802>.
- Uddin, L.Q., Menon, V., 2009. The anterior insula in autism: under-connected and under-examined. *Neurosci. Biobehav. Rev.* 33, 1198–1203. <http://dx.doi.org/10.1016/j.neubiorev.2009.06.002>.
- Uddin, L.Q., Kelly, A.M., Biswal, B.B., Castellanos, F.X., Milham, M.P., 2009. Functional connectivity of default mode network components: correlation, anticorrelation, and causality. *Hum. Brain Mapp.* 30, 625–637. <http://dx.doi.org/10.1002/hbm.20531>.
- Uddin, L.Q., et al., 2013. Salience network-based classification and prediction of symptom severity in children with autism. *JAMA Psychiatry* 70, 869–879. <http://dx.doi.org/10.1001/jamapsychiatry.2013.104>.
- Vernet, M., Quentin, R., Chanes, L., Mitsumasu, A., Valero-Cabre, A., 2014. Frontal eye field, where art thou? Anatomy, function, and non-invasive manipulation of frontal regions involved in eye movements and associated cognitive operations. *Front. Integr. Neurosci.* 8, 66. <http://dx.doi.org/10.3389/fnint.2014.00066>.
- Zhang, D., Raichle, M.E., 2010. Disease and the brain's dark energy. *Nat. Rev. Neurol.* 6, 15–28. <http://dx.doi.org/10.1038/nrneurol.2009.198>.
- Zoghbi, H.Y., Bear, M.F., 2012. Synaptic dysfunction in neurodevelopmental disorders associated with autism and intellectual disabilities. *Cold Spring Harb. Perspect. Biol.* 4. <http://dx.doi.org/10.1101/cshperspect.a009886>.